



Computer modeling, docking, spectroscopic analysis, and antibacterial testing of metal chelates with dioxatetraaza ligand.

Ehab M. Zayed*¹, Wael A. El-Sayed^{2,3}, Hayam A. Abd El Salam¹ Gehad G. Mohamed^{4,5}

¹Green Chemistry Department, National Research Centre, 33 El-Bohouth St. (former El Tahrir St.), P.O. 12622, Dokki, Giza, Egypt

²Department of Chemistry, College of Science, Qassim University, Buraidah 51452, Saudi Arabia

³Photochemistry Department, National Research Centre, Cairo 12622, Egypt

⁴Chemistry Department, Faculty of Science, Cairo University, Giza 12613, Egypt

⁵Nanoscience Department, Basic and Applied Sciences Institute, Egypt-Japan University of Science and Technology, New Borg El Arab, Alexandria, 21934, Egypt



Abstract

The goal of our current research is to create novel compounds of Co(II), Ni(II), Cu(II), Cr(III), Fe(III) and Zn(II) metal ions from heterocyclic dioxatetraaza ligand by the reaction of N1,N1'-(ethane-1,2-diyl)bis(ethane-1,2-diamine) with 2,2'-(ethane-1,2-diylbis(oxy))dibenzaldehyde to find out combating agent against microorganism diseases. Various physicochemical and spectroscopic techniques, including FT-IR, 1H and magnetic susceptibility, mass spectrometry, TGA, and others, were used to precisely characterize the synthesized compounds. These techniques suggested that the complexes' octahedral geometry was formed by epoxy oxygen atoms, azomethine nitrogen atoms of the dioxatetraaza ligand, and oxygen from the water molecules. The compounds' in vitro antibacterial activity against two bacterial and fungal pathogens was evaluated using the serial dilution method. Theoretical molecular docking was used to confirm these findings.

Keywords: dioxatetraaza; physicochemical technique; Microorganism; Antimicrobial activity; Transition metal chelates

Introduction

In the past, microbial diseases have been responsible for a sizably high number of mortality worldwide. Since the discovery of penicillin as a strong antibacterial agent in the 1940s, the use of numerous natural and synthetic antibiotics has fortunately significantly aided human health[1]. The rapid proliferation of infectious diseases and the rise in the number of multidrug-resistant microorganisms make it difficult to treat bacterial infections. Due to shortcomings including antagonistic interactions, a lack of diversity, and a lack of disease-modifying agents in hospitals, currently existing treatments have lost their efficacy, contributing to an ongoing global epidemic that has a negative impact on people's health and the economy of their countries[2-5]. Therefore, one of the most important tasks in medicinal chemistry today is the hunt for new, highly effective therapeutic molecules with minimal side effects. As a result, we determined that transition metal complexes of dioxatetraaza ligands

offer a great possibility for the study and development of new active antimicrobial medicines that can efficiently create pathogenic deformities with the fewest adverse effects [5-7]. The structural diversity and activity of metal complexes are increased when dioxatetraaza ligands are bound to transition metal ions. This encourages researchers to create new metal complexes using dioxatetraaza ligands. They can alter the charge, substitution kinetics, lipophilicity, and mode of action of biological targets by using a variety of three-dimensional geometries and potentially infinite design options for their coordination sphere. They are widely used as analytical reagents, fluorescent materials, and polymer coating pigments for coating polymers due to their prominence as chelation abilities, reactivity, preparative accessibilities, and flexibility as they contain -NH-C=O group in proximity to isocyanic acid, which makes them suitable for coordination with transition metal atoms [8-11], transition metal complexes with

*Corresponding author e-mail: ehab_zayed2002@yahoo.com.

Receive Date: 15 October 2023, Revise Date: 23 November 2023, Accept Date: 27 November 2023

DOI: 10.21608/EJCHEM.2023.238209.8653

©2023 National Information and Documentation Center (NIDOC)

dioxatetraaza occupy a main position in medicinal chemistry. Biological uses of transition metal complexes with dioxatetraaza ligands include antifungal [12], antibacterial, anticancer, antiplatelets, and antimalarial [13]. antioxidants, antiradicals, antitubercular [14], anti-inflammatory, etc. Additionally, transition metal complexes with dioxatetraazaligand are gaining attention from researchers due to their variety of pharmacological and biological applications, but it is challenging for them to develop substantial pharmaceutical compounds with improved pharmacological applications. They are widely used as analytical reagents, fluorescent materials, and polymer coating pigments for coating polymers due to their prominence as chelation abilities, reactivity, preparative accessibilities, and flexibility as they contain -NH-C=O group in proximity to azomethine group, which makes them suitable for coordination with transition metal atoms [15-19].

Experimental

The earlier work covered every detail in the experimental portion. [20]

Materials and reagents

All chemicals were of the purest and highest analytical reagent grade (AR). $\text{CoCl}_2 \cdot 6\text{H}_2\text{O}$ (BDH), $\text{CuCl}_2 \cdot 2\text{H}_2\text{O}$ (BDH), $\text{NiCl}_2 \cdot 6\text{H}_2\text{O}$ (BDH), $\text{ZnCl}_2 \cdot 2\text{H}_2\text{O}$ (BDH), and $\text{CrCl}_3 \cdot 6\text{H}_2\text{O}$ (BDH) was provided by Prolabo. Without additional purification, organic solvents like EtOH and DMF were employed as received.

Solutions

In order to make prepared metal complex stock solutions, a carefully weighed quantity of the complex was dissolved in EtOH and DMF (1:3 v/v ratio) to obtain $1 \times 10^{-3}\text{M}$. We created a stock solution of the ligand and its metal complexes ($5 \times 10^{-4}\text{M}$) through dilution in order to examine their UV-Vis spectra.

Synthesis of dioxatetraaza Ligand

Condensation of 2-[2-(2-formylphenoxy)ethoxy]benzaldehyde with triethylene tetra amine gives the corresponding cyclic Schiff base as identified by IR, $^1\text{H-NMR}$ and mass spectra. Filtering was used to collect the solid that formed after cooling, and compound 1 was created as buff crystals by recrystallizing toluene. Yield: 81%. M.p.: 110°C . FT-IR (KBr, cm^{-1}): 3036m $\nu(\text{NH})$, 829s $\delta(\text{NH})$, 1597sh $\nu(\text{HC}=\text{N})$ and 1049m $\nu(\text{C}-\text{O}-\text{C})$. $^1\text{H-NMR}$ (500 MHz, DMSO): $2.654\sim 2.975$, (m, 6H, -NH-CH₂); 4.429 (m, 2H, -OCH₂); 3.545 (m, 1H, NH); $6.840\sim 7.977$ (m, 4H, ArH). MS (EI, m/z): f, 380 (M⁺), calc, 380 g/mol. Anal. Calcd. for $\text{C}_{22}\text{H}_{28}\text{N}_4\text{O}_2$: C, 69.45; H, 7.42; N, 14.73. Found: C, 69.40; H, 7.38; N, 14.69.

Synthesis of metal complexes

The Ni(II), Co(II), Cu(II), Cr(III), Zn(II) and Fe(III) Equivalent amounts of the ligand and metal chloride ratio were mixed (1M: 1L molar ratio) in EtOH, which was then heated for 3h. to create complexes. After filtering the resulting precipitates, the filtrates were repeatedly washed with hot ethanol until they were clear, yielding, respectively, 96, 80, 89, 82, 83, and 80 percent of Co(II), Ni(II), Cu(II), Zn(II), Cr(III), and Fe(III) complexes. The appropriate products were then dried in a desiccator over anhydrous CaCl_2 . $[\text{Cr}(\text{L})(\text{H}_2\text{O})_2]\text{Cl}_3$; yield 83%; m.p. 118°C ; Brown solid. Anal. Calc. for $\text{C}_{22}\text{H}_{32}\text{Cl}_3\text{CrN}_4\text{O}_4$ (%): C, 45.96; H, 5.61; N, 9.75; Cl, 18.50; M, 9.04. Found (%): C, 45.92; H, 5.57; N, 9.71; Cl, 18.45; M, 9.01. FT-IR (KBr, v , cm^{-1}): 2920m $\nu(\text{NH})$, 815m $\delta(\text{NH})$, 1604sh $\nu(\text{HC}=\text{N})$, 1040m $\nu(\text{C}-\text{O}-\text{C})$, 519wv $\nu(\text{M}-\text{O})_{\text{H}_2\text{O}}$, 540sv $\nu(\text{M}-\text{O})_{\text{ether}}$, 467sv $\nu(\text{M}-\text{N})_{\text{azo}}$. μ_{eff} (BM) 3.48; Λ_{m} ($\Omega^{-1}\text{mol}^{-1}\text{cm}^2$) 161.8.

$[\text{Fe}(\text{L})(\text{H}_2\text{O})_2]\text{Cl}_3$; yield 83%; m.p. 110°C ; Yellowish Brown solid. Anal. Calc. for $\text{C}_{22}\text{H}_{32}\text{Cl}_3\text{FeN}_4\text{O}_4$ (%): C, 45.66; H, 5.57; N, 9.68; Cl, 18.38; M, 9.65. Found (%): C, 45.62; H, 5.52; N, 9.64; Cl, 18.34; M, 9.61. FT-IR (KBr, v , cm^{-1}): 2932sh $\nu(\text{NH})$, 833m $\delta(\text{NH})$, 1610sh $\nu(\text{HC}=\text{N})$, 1039sh $\nu(\text{C}-\text{O}-\text{C})$, 470wv $\nu(\text{M}-\text{O})_{\text{H}_2\text{O}}$, 520sv $\nu(\text{M}-\text{O})_{\text{ether}}$, 462sv $\nu(\text{M}-\text{N})_{\text{azo}}$. μ_{eff} (BM) 5.34; Λ_{m} ($\Omega^{-1}\text{mol}^{-1}\text{cm}^2$) 166.0.

$[\text{Co}(\text{L})(\text{H}_2\text{O})_2]\text{Cl}_2$; yield 96%; m.p. 280°C ; Dark Greensolid. Anal. Calc. for $\text{C}_{22}\text{H}_{32}\text{Cl}_2\text{CoN}_4\text{O}_4$ (%): C, 48.36; H, 5.90; N, 10.25; Cl, 12.98; M, 10.79. Found (%): C, 48.32; H, 5.85; N, 10.22; Cl, 12.95; M, 10.72. FT-IR (KBr, v , cm^{-1}): 2980s $\nu(\text{NH})$, 800s $\delta(\text{NH})$, 1643sh $\nu(\text{HC}=\text{N})$, 1056m $\nu(\text{C}-\text{O}-\text{C})$, 443wv $\nu(\text{M}-\text{O})_{\text{H}_2\text{O}}$, 513sv $\nu(\text{M}-\text{O})_{\text{ether}}$, 417sv $\nu(\text{M}-\text{N})_{\text{azo}}$. μ_{eff} (BM) 5.02; Λ_{m} ($\Omega^{-1}\text{mol}^{-1}\text{cm}^2$) 98.7.

$[\text{Ni}(\text{L})(\text{H}_2\text{O})_2]\text{Cl}_2$; yield 80%; m.p. 104°C ; Brown solid. Anal. Calc. for $\text{C}_{22}\text{H}_{32}\text{Cl}_2\text{NiN}_4\text{O}_4$ (%): C, 48.38; H, 5.91; N, 10.26; Cl, 12.98; M, 10.75. Found (%): C, 48.35; H, 5.87; N, 10.22; Cl, 12.92; M, 10.71. FT-IR (KBr, v , cm^{-1}): 2928m $\nu(\text{NH})$, 822s $\delta(\text{NH})$, 1590sh $\nu(\text{HC}=\text{N})$, 1055sh $\nu(\text{C}-\text{O}-\text{C})$, 444sv $\nu(\text{M}-\text{O})_{\text{H}_2\text{O}}$, 522sv $\nu(\text{M}-\text{O})_{\text{ether}}$, 418wv $\nu(\text{M}-\text{N})_{\text{azo}}$. μ_{eff} (BM) 3.44; Λ_{m} ($\Omega^{-1}\text{mol}^{-1}\text{cm}^2$) 104.3.

$[\text{Cu}(\text{L})(\text{H}_2\text{O})_2]\text{Cl}_2$; yield 89%; m.p. 250°C ; Brown solid. Anal. Calc. for $\text{C}_{22}\text{H}_{32}\text{Cl}_2\text{CuN}_4\text{O}_4$ (%): C, 47.96; H, 5.85; N, 10.17; Cl, 12.87; M, 11.53. Found (%): C, 47.92; H, 5.81; N, 10.12; Cl, 12.82; M, 11.50. FT-IR (KBr, v , cm^{-1}): 3067m $\nu(\text{NH})$, 810s $\delta(\text{NH})$, 1601sh $\nu(\text{HC}=\text{N})$, 1045m $\nu(\text{C}-\text{O}-\text{C})$, 517sv $\nu(\text{M}-\text{O})_{\text{H}_2\text{O}}$, 530sv $\nu(\text{M}-\text{O})_{\text{ether}}$, 470sv $\nu(\text{M}-\text{N})_{\text{azo}}$. μ_{eff} (BM) 1.77; Λ_{m} ($\Omega^{-1}\text{mol}^{-1}\text{cm}^2$) 100.7.

$\text{Zn}(\text{L})(\text{H}_2\text{O})_2]\text{Cl}_2$; yield 82%; m.p. 170°C ; Honey Brown solid. Anal. Calc. for $\text{C}_{22}\text{H}_{32}\text{Cl}_2\text{ZnN}_4\text{O}_4$ (%): C, 47.80; H, 5.83; N, 10.14; Cl, 12.83; M, 11.83. Found (%): C, 47.75; H,

5.80; N, 10.10; Cl, 12.79; M, 11.78. FT-IR (KBr, ν , cm^{-1}): 2928 $\nu(\text{NH})$, 830 $\delta(\text{NH})$, 1605 $\nu(\text{HC}=\text{N})$ and 1053 $\nu(\text{C}-\text{O}-\text{C})$, 471 $\nu(\text{M}-\text{O})_{\text{H}_2\text{O}}$, 511 $\nu(\text{M}-\text{O})_{\text{ether}}$, 460 $\nu(\text{M}-\text{N})_{\text{azo}}$. μ_{eff} (BM) diamagnetic; Λ_{m} ($\Omega^{-1}\text{mol}^{-1}\text{cm}^2$) 100.3.

Spectrophotometric studies

Over the wavelength range of 200 to 700 nm, the absorption spectra of 1×10^{-4} M solutions of dioxatetraaza ligand and metal complexes were measured.

Molecular docking

Both Auto Dock 4.2 and docking calculations with the ligand (designed drug) atoms subjected to Gasteiger partial charges were used. Calculations of the ligand-protein pattern were done. Clarifying rotatable bonds and linking nonpolar hydrogen atoms. Kollman unified atom type charges and solvation parameters were added using the Auto Dock tools after the introduction of fundamental hydrogen atoms [21]. The distance-dependent dielectric functions and the Auto Dock parameter set, respectively, were used to calculate the van der Waals and electrostatic terms. The Lamarckian genetic algorithm was used to mimic docking using the Solis and Wets local search approach. The beginning location, orientation, and torsion of the ligand molecule were all identified.

Biological activity

Testing for new antibacterial and antifungal compounds' susceptibility to microbes can be used to foretell how a treatment will work. The Clinical and Laboratory Standards Institute (CLSI) states that one of the manual AST techniques that is most frequently employed in clinical microbiology laboratories is the agar disc diffusion test [22], and it was used to test the evaluated substances for their *in vitro* antibacterial and antifungal activity. The main advantages include the test's simplicity, reproducibility, ease of customizing Antibacterial and Antifungal discs, and ability to be used as a screening test for a range of Antibacterial and Antifungal isolates. Mueller-Hinton agar plates are inoculated with tested antibacterial and antifungal inoculums that are standardized species; *Aspergillus flavus* (Fungus) (7BOP), *Candida albicans* (Fungus) (5k04), *Escherichia coli* (G-) (3t88), and *Staphylococcus aureus* (G+) (3ty7) are examples of host organisms that can be used to attach ligand and complexes (guests). Each disc was placed on the inoculated agar surface using commercially prepared paper discs (about 6 mm in diameter) impregnated with 100 μL of the required concentration of the tested drug. According to appropriate guidelines, agar plates are incubated for 16–24 hours at 35–37°C (CLSI 2018a; EUCAST 2019b). The diameter of the clear inhibition zones

surrounding each compound-impregnated disc is then measured in millimetres and factored into the outcome. This is done by hand while holding a ruler against the back of the inverted agar plate [23–25]. Tetracycline and amphotericin B were utilized as reference drugs standard for Gram-positive, Gram-negative, and fungal activities, whereas DMSO was employed as negative control. The outcomes of all the inoculation plates were examined in a table after 35°C incubation. The MIC values have an inverse relationship with the inhibitory zone. The larger the zone of growth inhibition, the lower the antimicrobial medication concentration required to stop the growth. However, it is important to consider a compound's diffusibility [26].

Computational methodology

Gaussian09 software was used to calculate the ligand's ideal structural geometry using the Ground state, DFT, B3LYP, and 3-21G. Gauss View, a molecular visualisation programme, was used to display Gaussian files [27]. In the view of compounds in the gas phase, the numerical pattern was consistent with the HOMO-LUMO energies used to construct the DFT/B3LYP quantum chemical parameters. Calculations were made for coordinating group charges, significant bond lengths, bond angles, dihedral angles, and excitation energy in optimised structures.

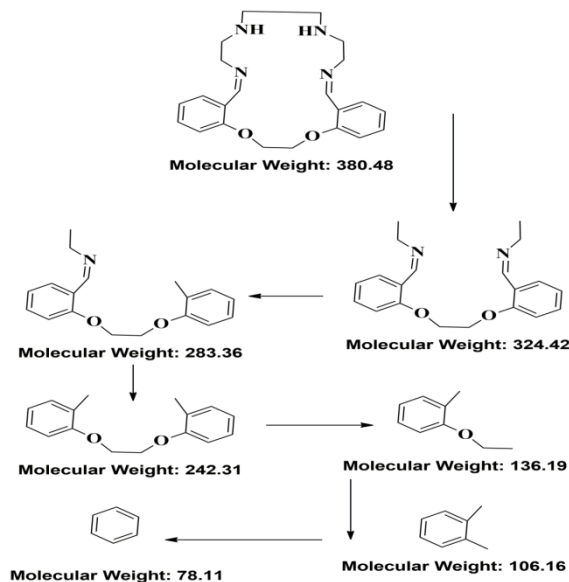
Results and discussion

The synthesis of dioxatetraaza cyclic ligand was carried out by reacting $\text{N1,N1'-(ethane-1,2-diyl)bis(ethane-1,2-diamine)}$ with $2,2'-(ethane-1,2-diylbis(oxy))dibenzaldehyde$ in hot methanol with the addition of 0.1 mL of glacial acetic acid. Further, complexation of the ligand was carried out from the reaction of metal(II) and metal(III) chlorides with synthesized dioxatetraaza ligand in 1:1 molar ratio. The analytical techniques revealed that synthesized dioxatetraaza ligand was bonded to metal ions *via* the azomethine nitrogen atoms, etheric oxygen atoms and NH atoms resulting in octahedral geometry. The compounds were examined by several spectral and physical techniques to ascertain the geometry of the complexes and other characteristic data. With the exception of DMF and DMSO, the compounds were not soluble in the majority of solvents.

Mass spectral study

To support the above-proposed structure, the mass spectrum of the dioxatetraaza ligand was examined and recorded at 70 eV. The molecular ion of the dioxatetraaza ligand (molar mass = 380.22 g/mol) is referenced by a peak at $m/z = 380$ amu. This result confirmed the suggested empirical formula of the dioxatetraaza ligand as indicated from elemental analyses. The primary molecular ion and its putative

fragment ions are produced by the dioxatetraaza ligand's cleavage of various bonds in various places, as indicated in Scheme 1. The mass spectrum showed fragment ions at $m/z = 324.42$, 283.36 , 242.31 , 136.19 , 106.16 and 78.11 amu which may be assigned to $C_{20}H_{24}N_2O_2$, $C_{18}H_{21}NO_2$, $C_{16}H_{18}O_2$, $C_9H_{12}O$, C_8H_{10} and C_6H_6 fragments



Scheme 1. Mass fragmentation of ligand

IR spectral study

With the exception of a few modest shifts and intensity changes of a few vibration peaks brought on by various metal (III/II) ions, the IR spectra of the metal complexes are similar to one another, showing that the metal complexes have a similar structure. The most significant IR bands of Schiff base ligand and its metal complexes along with their likely intensities were given in the experimental part. The ligand has many sites for coordination, which resulted in a variety of coordination modes. When compared to the free ligand, the IR spectra of all complexes exhibit a shift in the band of the azomethine N, $\nu(C=N)$, from 1590 to 1643 (1597 cm^{-1} in the free ligand) confirming its involvement in chelation [28]. The band due to the etheric O, $\nu(C-O-C)$, found at 1049 cm^{-1} in the free ligand IR spectrum was found at 1039 – 1056 cm^{-1} in the metal complexes IR spectra. This shift can be assigned to the participation of etheric oxygen in the coordination. The shift in the $\nu(NH)$ or $\delta(NH)$ towards lower or higher frequencies can be attributed to the change in the skeleton of the Schiff base ligand due to chelation to metal ions [29]. Additionally, the new bands between the areas of 417 – 470 cm^{-1} , 511 – 540 cm^{-1} and 417 – 519 cm^{-1} can be attributed to $\nu(M-N)$, $\nu(M-O)$ etheric and $\nu(M-$

of the parent Schiff base ligand. The suggested scheme lists potential fragment ion structural equations together with potential names using the IUPAC system. Thermal degradation of the dioxatetraaza ligand examined at two distinct heating rates has corroborated these fragmentations.

O)water, respectively [30–32]. This leads us to the conclusion that the complexes' coordination geometry, which includes two nitrogen and two oxygen donors of the macrocyclic Schiff base ligand and the two oxygen atoms from water molecules, is distorted octahedral, indicating that the Schiff base functions as a tetradentate neutral ligand.

¹H-NMR spectral study

Schiff base's ¹H-NMR spectrum in *d*₆-DMSO exhibited signal at 8.53 ppm which assigned to azomethine CH=N proton. As a result of its participation in the chelation mode, its position in the Zn(II) complex has shifted to 7.95 ppm. The signal found at 3.55 ppm which assigned to NH proton for the Schiff base ligand, as a result of change in the carbon skeleton due to chelation, its position in the Zn(II) complex ¹H-NMR spectrum has shifted to 3.32 ppm. Additionally, at 6.84 – 7.98 ppm in the free ligand and 7.12 – 7.15 ppm in the Zn(II) complex, numerous signals attributed to aromatic ring protons were detected [33].

Thermogravimetric analysis study

Table 1 contains the results of the thermogravimetric study of the Schiff base ligand and its metal complexes. The experimental findings showed that ligand degradation follows a complicated mechanism and occurs in a number of phases. For the Schiff basedioxatetraaza ligand, the first two estimated mass losses of 13.50% (calcd. 13.42%) in the range of 175 – 405 °C may be attributed to the liberation of $3NH_3$ as gases, and in the following stages the remaining organic part ($C_{21}H_{19}$ molecule), CO_2 and $\frac{1}{2}N_2$ gases are lost with an estimated mass loss of 86.50% (calcd. 86.58%) with a complete decomposition within the temperature range from 410 to ~ 935 °C. In contrast, the Fe(III), Co(II), and Cu(II) chelates displayed four steps of decomposition between 25 – 790 °C, 45 – 630 °C, and 35 – 830 °C. These decomposition can be attributed to the loss of water molecules, anions present in the outer coordination sphere and decomposition of the Schiff base ligand to gases (Table 1). The overall weight losses of 86.90% (calculated as 86.76%), 84.91% (calculated as 84.91%), and 84.91% (calculated as 86.76%), respectively, were reported for Fe(III), Co(II) and Cu(II) complexes. FeO (estimated mass loss = 13.10 ; calculated mass loss = 13.24), CoO (estimated mass loss = 15.09 ; calculated mass loss = 14.69), and CuO (estimated mass loss = 15.29 ; calculated mass

loss = 15.46) were the metal oxides left over after the complexes broke down.

The Coats-Redfern relation (equation 1) is used to graphically analyse the activation energies (E^*), enthalpies (H^*), Gibbs free energy change of the decomposition (G^*) and entropies (S^*) of the thermodynamic processes that lead to the breakdown of dehydrated complexes:

$$\log \left[\frac{\log \{W_f / (W_i - W_f)\}}{T^2} \right] = \log \left[\frac{AR}{\theta E^*} \left(1 - \frac{2RT}{E^*} \right) \right] - \frac{E^*}{2.303 RT} \quad (1)$$

Where W_f is the mass loss at reaction completion, R is the gas constant, and θ is the heating rate W is the

mass loss up to temperature T , E^* is the activation energy in $\text{kJ}\cdot\text{mol}^{-1}$, and $(1 - (2RT/E^*)) \cong 1$. The slope from which the left side of equation (1) is plotted against $1/T$ can be used to compute E^* , and the intercept can be used to get A (Arrhenius factor). According to the Coats-Redfern equation [34], the complexes' high activation energies represent their thermal stability, and the fact that all of the complexes' activation entropies are negative means that the breakdown reactions happen more slowly than they would normally.

Table 1. Thermoanalytical results (TG and DTG) for Schiff base dioxatetraaza ligand and its metal complexes

Compound	TGrange/ $^{\circ}\text{C}$	DTGmax/ $^{\circ}\text{C}$	n*	Mass loss (Total mass loss)	Assignment	Metallic Residue/%
H_2L	175-405	320.383	2	13.42(13.50)	-Loss of 3NH_3	-
	410-935	421.640,861	3	86.58(86.50),100(100)	-Loss of $\text{CO}_2, \frac{1}{2}\text{N}_2$ and C_2H_{19}	
$[\text{Fe}(\text{H}_2\text{L})(\text{H}_2\text{O})_2]\text{Cl}_3$	25-350	76,296	2	12.82(12.76)	-Loss of HCl, NO and $\frac{1}{2}\text{H}_2$	FeO
	350-465	394	1	16.04(15.99)	-Loss of 2HCl and $\frac{1}{2}\text{N}_2$	
	465-790	671	1	57.90(58.15)86.76(86.90)	-Loss of $\text{C}_2\text{H}_2\text{N}_2$	
$[\text{Co}(\text{H}_2\text{L})(\text{H}_2\text{O})_2]\text{Cl}_2$	45-350	81,317	2	18.43(18.42)	-Loss of $2\text{HCl}, \text{CH}_4$ and $\frac{1}{2}\text{H}_2$	CoO
	350-630	433,568	2	66.88(66.49), 85.31(84.91)	-Loss of $4\text{NH}_3, \text{CO}$ and C_{20}H_5	
$[\text{Cu}(\text{H}_2\text{L})(\text{H}_2\text{O})_2]\text{Cl}_2$	35-125	62	1	5.44(5.59)	-Loss of N_2	CuO
	125-320	212	1	10.20(10.01)	-Loss of HCl and $\frac{1}{2}\text{O}_2$	
	320-480	346	1	17.98(18.04)	-Loss of $\text{HCl}, 2\text{NH}_3, \text{CH}_4$ and 3H_2	
	480-830	590	1	50.92(51.07), 84.54(84.71)	-Loss of $\text{C}_{21}\text{H}_{10}$	

Table 2. Calculated quantum chemical parameters of dioxatetraaza ligand.

Parameter	
E_{HOMO} (a.u.)	-0.23083
E_{LUMO} (a.u.)	0.00838
μ (D)	-39.4251
T.E (a.u.)	-1217.85
ΔE (a.u.)	0.23921
χ (a.u.)	0.111225
η (a.u.)	0.119605
σ (a.u.) ⁻¹	8.360854
Pi (a.u.)	-0.11123
S (a.u.) ⁻¹	4.180427
ω (a.u.)	0.05171607
ΔN_{max}	0.929936039

Molecular modeling

The geometrical geometry of the dioxatetraaza ligand as well as a theoretical tool for molecular modeling was both created using the Gaussian09 program. The electronic structure of the dioxatetraaza ligand can be determined using the separation in orbital energy between EHOMO and ELUMO [19] Examples of the molecular orbitals of the free dioxatetraaza ligand show that the donor atoms—nitrogen of the azomethine group and oxygen of the epoxy group—that are employed to donate to metal ion acceptors were mainly focused

on the LUMO, HOMO, and charge distribution. (Figure 1). Table 2 contains chemical calculations and the data that were obtained. The dipole moment (μ) and other parameters like the HOMO-LUMO energy gap (E), chemical potential (Pi), absolute electronegativity (E), absolute hardness (H), additional electronic charge (ΔN_{max}), absolute softness (S), and global softness (E) were calculated. The first derivative of the energy with respect to an applied electric field was utilized to evaluate and explain the proposed structure. One of the theoretical models used was the energy gap (E), a significant stability parameter that aids in explaining the structures and conformational barriers in many compounds. Values were derived using previously published equations. [35-37]. The free dioxatetraaza ligand was revealed to have the following properties following the determination of all the parameters (Table 2). The soft property of the free ligand was used to infer the flexible reactions to metal ions.

Atomic charges, bond lengths and bond angles

Atomic charge calculations provide the foundation of quantum mechanical computation [38]. In the supplemental material (Supplementary Tables S1 and S2), the results of the charges population research with optimised geometry used to calculate the total atomic charge are presented. The two

promising atoms in the dioxatetraaza ligand are nitrogen and oxygen. This demonstrates that a high electron density, particularly in the region surrounding dioxatetraaza, is what causes the more active site, which promises to produce chelation.

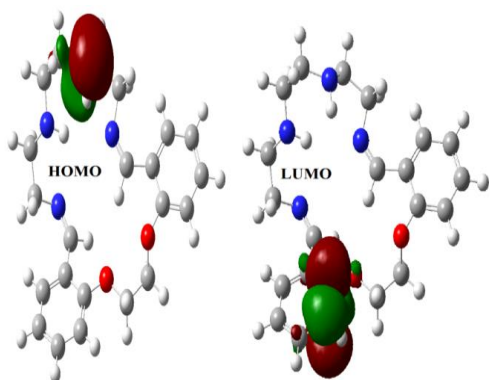


Figure 1. LUMO and HOMO patterns of studied dioxatetraaza ligand.

Figure 2 showed the numbering sequence of the dioxatetraaza ligand structure. It may be demonstrated that nitrogen and oxygen atoms melt at higher temperatures than atoms of other sizes do, suggesting that these atoms may be able to produce coordination compounds by chelating with metal atoms. The ideal coordination sites in the dioxatetraaza ligand were predicted using the Mulliken method and molecular electrostatic potential analysis. All of them indicate how brittle the bond is and imply that it will be the first to fail (Supplementary Tables S1 and S2). This theory fit in with the previous discussion and was consistent with how mass fragmentation and heat deterioration work.

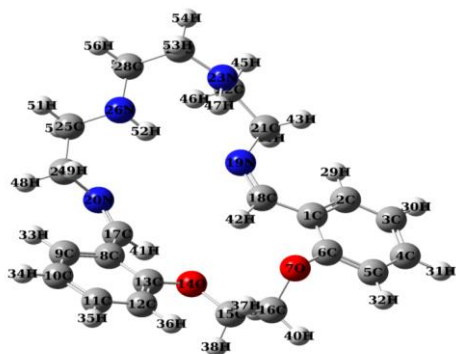


Figure 2. Optimized ligand structure with numbering system.

Characterization of metal complexes

Figure 2 illustrated how the dioxatetraaza ligand structure was numbered. We can show that the

melting temperatures of nitrogen and oxygen atoms are greater than those of other atoms of a similar size, indicating that these atoms would be able to form coordination compounds by chelating with metal atoms. The ideal coordination sites for the dioxatetraaza ligand were determined using the Mulliken method and a study of the molecular electrostatic potential. The relationship is clearly tenuous, and all of them (Supplementary Tables S1 and S2) imply that it will be the first to fall apart. The implications of mass fragmentation and heat deterioration were supported by this theory, which also added to the earlier discussion. [39].

Molecular Docking

With auto Dock, you can see the results of testing up close and discuss and demonstrate the biological benefits of ligands. Examples of hosts that can be utilized to attach ligands (guests) include *Aspergillus flavus* (Fungus)(7BOP), *Candida albicans* (Fungus)(5k04), *Escherichia coli* (G-)(3t88), and *Staphylococcus aureus* (G+)(3ty7). Figures 5-8 demonstrate that HB plots are capable of producing findings that are comparable and reveal a high level of interaction with all receptors. All proteins possessed inter hydrogen bonds that could be seen, according to calculations. The interactions between docking molecules can be depicted in three dimensions. Utilizing three-dimensional graphics, the mechanism of interaction within docking molecules may be demonstrated (Figures 3-6).

The interaction between the ligand and the amino acids of the protein in the following bacteria was shown to be largely mediated by hydrogen bonds. For *Candida albicans* fungus(5k04), An amino acid in the protein reacted with the ligand to cause the H-bond reaction: 5k04-h/5k04/B/ASN`117/2HD2- with H bond length 2.3 Å, 5k04-h/5k04/B/TYR`124/OH- with H bond length 3.3 Å, 5k04-h/5k04/B/ASN`117/ND2- with H bond length 2.5 Å, 5k04-h/5k04/B/GLU`63/OE1- with H bond length 3.4 Å and 5k04-h/5k04/B/PHE`112/O- with hydrogen bond length 2.7 Å, with binding energy = -10.9 kcal mol⁻¹ (Figures 3-6).

For *Aspergillus flavus* fungus(7BOP): amino acid of protein reacted with ligand by H-bond: 1- 7bop-h//A/GLU`205/OE2- with H bond length 2 Å, 7bop-h//A/GLU`205/OE2- with hydrogen bond length 3.5 Å, 7bop-h//A/TRP`291/HE1- with hydrogen bond length 2.7 Å and 7bop-h//A/SER`389/O- with hydrogen bond length 3.1 Å,

with binding energy = $-8.6 \text{ kcal mol}^{-1}$ (Figures 3–6).

For *Staphylococcus aureus*(G+)(3ty7), the amino acid of the protein combines with the ligand via a hydrogen bond: 3ty7-correct-A-h//A/GLU`49/OE1–with hydrogen bond length 3.3 \AA , 3ty7-correct-A-h//A/GLU`49/OE1–with H bond length 2.6 \AA , 3ty7-correct-A-h//A/GLU`49/OE2–with hydrogen bond length 3.5 \AA , 3ty7-correct-A-h//A/GLU`49/OE2–with H bond length 1.9 \AA , with binding energy = $-5.8 \text{ kcal mol}^{-1}$.

For *Escherichia coli*(G-)(3t88): ligand reacted with amino acids of protein by H-bond as follow: 3t88-correct-A-h/A1/A/SER`84/HG–with hydrogen bond length 2.2 \AA , 3t88-correct-A-h/A1/A/VAL`44/O–with H bond length 3.1 \AA and 3t88-correct-A-h/A1/A/GLY`78/O–with hydrogen bond length 2.7 \AA , with binding energy = $-7.6 \text{ kcal mol}^{-1}$ (Figures 3–6).

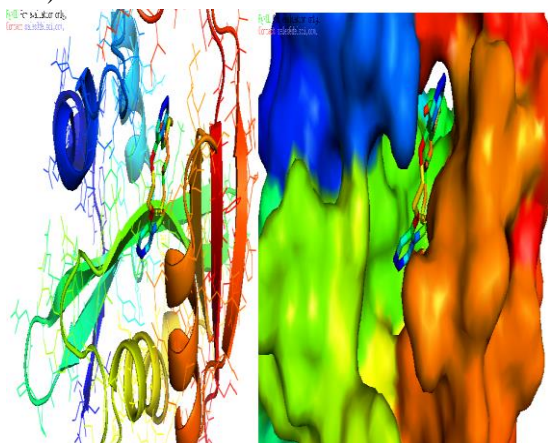


Figure 3. Three-dimensional plot of interaction of dioxatetraaza ligand with *Candida albicans* fungus(5k04) receptor.

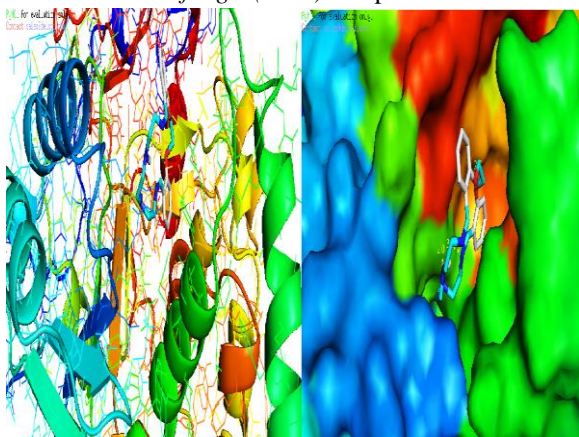


Figure 4. Three-dimensional plot of interaction of dioxatetraaza ligand with *Aspergillus flavus* fungus-7BOPreceptor

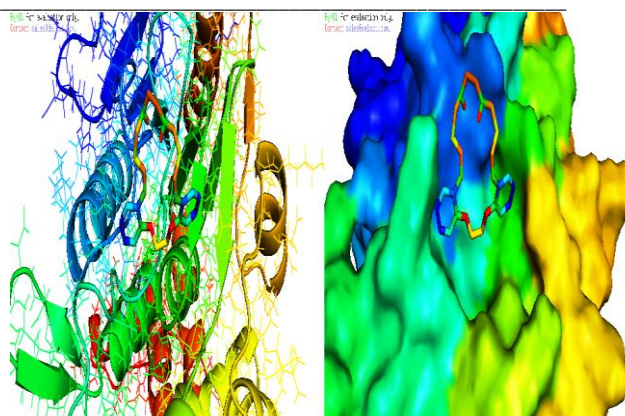


Figure 5. Three-dimensional plot of interaction of dioxatetraaza ligand with *Escherichia coli*(G-)-3t88receptor.

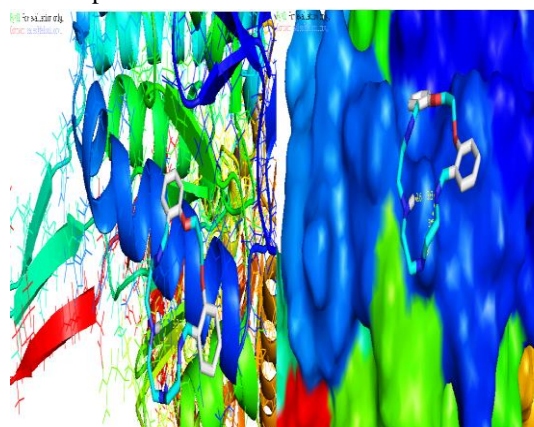


Figure 6. Three-dimensional plot of interaction of dioxatetraaza ligand with *Staphylococcus aureus*(G+)-3ty7receptor.

3.9. Antimicrobial activity

We used the serial dilution approach to assess all the compounds' in vitro antimicrobial (antibacterial and antifungal) activities against two fungal pathogens and four bacterial pathogens because the entire world is currently dealing with various illnesses brought on by microorganisms. The results were compared to the benchmarks amphotericin B and tetracycline for their relative antibacterial and antifungal properties.

The information gathered led to the following conclusions. The antibacterial activity of produced dioxatetraaza ligand and metal complexes is significantly influenced by the presence of the azomethine group ($-\text{C}=\text{N}-$). The research findings showed that metal complexes are more powerful than their corresponding dioxatetraaza ligand. The higher potency of metal complexes was explained by chelation theory and overtone's concepts, which showed that lipophilicity is an important factor in the increased activity of metal complexes. Chelation

enhances the capacity of the complex to pass through lipid membranes and decreases the polarizability and positive charge on the metal, which prevents the active site of microorganisms.

- Among the bacterial strains all complexes have more potency against *Staphylococcus aureus* and *E. coli* with ordered Cu(II), Ni(II) and Zn(II) are most highest complexes activity [40,41].

- All the synthetic compounds showed strong antifungal activity against *C. albicans* and *Aspergillus flavus*, with the most effective activity being seen in the complex ordered Cu(II) and Zn(II), and Co(II) and Ni(II) complexes are moderated one while Cr(III) complexes and Fe(III) are the least one.

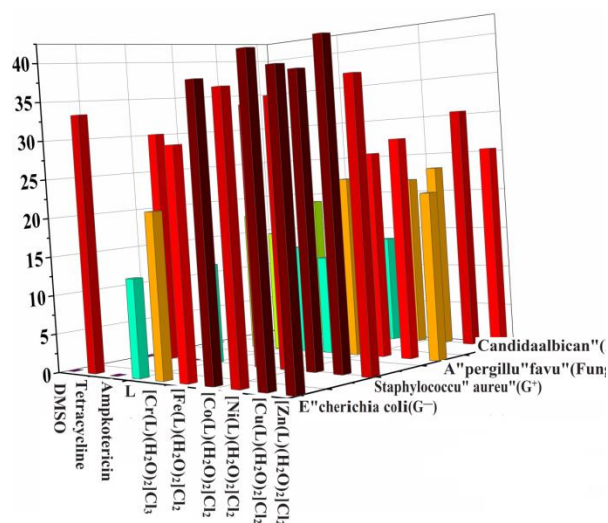


Figure 5. Biological activities of dioxatetraaza ligand and its metal complexes.

Conclusion

Dioxatetraaza ligand and its Co(II), Cu(II), Ni(II), Zn(II), Cr(III), and Fe(III) complexes were studied using physicochemical methods. Thermal measurements (TGA and DTG) revealed that the complexes were thermally stable up to 800 °C. DFT calculations were used to confirm that the octahedral geometry of the Co(II), Cu(II), Ni(II), Zn(II), Cr(III), and Fe(III) complexes was disclosed by combining magnetic susceptibility data with electronic spectra. All of the synthesized compounds demonstrated a weak to strong antibacterial impact when used against pathogenic bacteria species. The antimicrobial study also found that complexes' growth inhibitory effects were stronger than those of

their ligands. The higher antibacterial activity of the complexes is assumed to be caused by the hetero atoms present in them. To ascertain the antibacterial effectiveness, a docking research was conducted.

Reference

- [1] E.M. Zayed, G.G. Mohamed, A.M. Hindy, Transition metal complexes of novel Schiff base: Synthesis, spectroscopic characterization, and in vitro antimicrobial activity of complexes, *Journal of Thermal Analysis and Calorimetry* 120 (2015) 893-903.
- [2] R.M. Ramadan, A.K.A. Al-Nasr, A.F. Noureldeen, Synthesis, spectroscopic studies, antimicrobial activities and antitumor of a new monodentate V-shaped Schiff base and its transition metal complexes, *Spectrochimica Acta Part A: Molecular and Biomolecular Spectroscopy* 132 (2014) 417-422.
- [3] S. Matin, R. Khojasteh, Synthesis, characterization, and antibacterial activities of Cr (III), Co (III), Ni (II), and Mn (III) complexes of heptadentate Schiff base ligand derived from tris (2-aminoethyl) amine, *Russian Journal of General Chemistry* 85 (2015) 1763-1767.
- [4] A.O. Rajee, H.F. Babamale, A. Lawal, A.A. Aliyu, W.A. Osunniran, A.O. Sheriff, M. Lawal, J.A. Obaleye, Mn (II), Co (II), Ni (II), and Cu (II) complexes of amino acid derived Schiff base ligand: Synthesis, characterization and in-vitro antibacterial investigations, *Bulletin of the Chemical Society of Ethiopia* 35(1) (2021) 97-106.
- [5] W.M. Hassan, E.M. Zayed, A.K. Elkholy, H. Moustafa, G.G. Mohamed, Spectroscopic and density functional theory investigation of novel Schiff base complexes, *Spectrochimica Acta Part A: Molecular and Biomolecular Spectroscopy* 103 (2013) 378-387.
- [6] C. Chang, W. Chen, Y. Chen, Y. Chen, Y. Chen, F. Ding, C. Fan, H.J. Fan, Z. Fan, C. Gong, Recent progress on two-dimensional materials, *Acta Phys. Chim. Sin* 37(12) (2021) 2108017.
- [7] G.G. Mohamed, E.M. Zayed, A.M. Hindy, Coordination behavior of new bis Schiff base ligand derived from 2-furan carboxaldehyde and propane-1, 3-diamine. Spectroscopic, thermal, anticancer and antibacterial activity studies, *Spectrochimica Acta Part A:*

- Molecular and Biomolecular Spectroscopy 145 (2015) 76-84.
- [8] E.M. Zayed, G.G. Mohamed, W.M. Hassan, A.K. Elkholy, H. Moustafa, Spectroscopic, thermal, biological activity, molecular docking and density functional theoretical investigation of novel bis Schiff base complexes, *Applied Organometallic Chemistry* 32(7) (2018) e4375.
- [9] P. Mahadevi, S. Sumathi, A. Metha, J. Singh, Synthesis, spectral, antioxidant, in vitro cytotoxicity activity and thermal analysis of Schiff base metal complexes with 2, 2'-Bipyridine-4, 4'-dicarboxylic acid as co-ligand, *Journal of Molecular Structure* 1268 (2022) 133669.
- [10] V.P. Radha, S. Chitra, S. Jonekirubavathi, I.-M. Chung, S.-H. Kim, M. Prabakaran, Transition metal complexes of novel binuclear Schiff base derived from 3, 3'-diaminobenzidine: synthesis, characterization, thermal behavior, DFT, antimicrobial and molecular docking studies, *Journal of Coordination Chemistry* 73(6) (2020) 1009-1027.
- [11] A.M. Farag, H.H. Sokker, E.M. Zayed, F.A.N. Eldien, N.M. Abd Alrahman, Removal of hazardous pollutants using bifunctional hydrogel obtained from modified starch by grafting copolymerization, *International journal of biological macromolecules* 120 (2018) 2188-2199.
- [12] M.A. Mumit, M.A.-A.-A.-A. Islam, M.C. Sheikh, R. Miyatake, M.O.A. Mondal, M.A. Alam, Synthesis, characterization and antimicrobial activity of a bidentate NS Schiff base containing S-allyl dithiocarbamate and its complexes, *Journal of Molecular Structure* 1178 (2019) 583-589.
- [13] K.C.N.R. Pedro, I.E.P. Ferreira, C.A. Henriques, M.A.P. Langone, Enzymatic fatty acid ethyl esters synthesis using acid soybean oil and liquid lipase formulation, *Chemical Engineering Communications* 207(1) (2020) 43-55.
- [14] S. Rottenberg, C. Disler, P. Perego, The rediscovery of platinum-based cancer therapy, *Nature Reviews Cancer* 21(1) (2021) 37-50.
- [15] E.M. Zayed, A.M. Hindy, G.G. Mohamed, Molecular structure, molecular docking, thermal, spectroscopic and biological activity studies of bis-Schiff base ligand and its metal complexes, *Applied Organometallic Chemistry* 32(1) (2018) e3952.
- [16] E.M. Zayed, M.A. Zayed, M.A. Radwan, F.M. Alminderej, Synthesis, characterization, antimicrobial, and docking study of novel 1-(furan-2-yl)-3-(pyrrolyl) propenone-based ligand and its chelates of 3d-transition metal ions, *Applied Organometallic Chemistry* 36(1) (2022) e6489.
- [17] G.A. Eldeken, F.A. El-Samahy, E.M. Zayed, F.H. Osman, G.E. Elgemeie, Synthesis, biological activities and molecular docking analysis of a novel series of 1H-indeno [1, 2-b] quinoxalin-11-one derivatives, *Journal of Molecular Structure* 1261 (2022) 132929.
- [18] E.M. Zayed, G. Mohamed, Synthesis, spectroscopic, DFT and docking studies, molecular structure of new Schiff base metal complexes, *Egyptian Journal of Chemistry* 65(1) (2022) 633-644.
- [19] E.M. Zayed, M.A. Zayed, A.M. Hindy, G.G. Mohamed, Coordination behaviour and biological activity studies involving theoretical docking of bis-Schiff base ligand and some of its transition metal complexes, *Applied Organometallic Chemistry* 32(12) (2018) e4603.
- [20] F. Çelik, Y. Ünver, 1, 2, 4-Triazole derivative containing thiophen ring: Comparison of theoretical IR and NMR data with experimental, *Journal of the Indian Chemical Society* 99(6) (2022) 100455.
- [21] E.M. Zayed, F.A. El-Samahy, G.G. Mohamed, Structural, spectroscopic, molecular docking, thermal and DFT studies on metal complexes of bidentate orthoquinone ligand, *Applied Organometallic Chemistry* 33(9) (2019) e5065.
- [22] Y.M. Ahmed, G.G. Mohamed, New Tin (IV) Schiff base complexes: synthesis, characterization and antibacterial investigation, docking and theoretical studies, *Inorganic Chemistry Communications* 144 (2022) 109864.
- [23] E.M. Zayed, G.G. Mohamed, H.A. Abd El Salam, Ni (II), Co (II), Fe (III), and Zn (II) mixed ligand complexes of indoline-dione and naphthalene-dione: Synthesis, characterization, thermal, antimicrobial, and molecular modeling studies, *Inorganic Chemistry Communications* 147 (2023) 110276.

- [24] S. Kumar, J. Devi, A. Dubey, D. Kumar, D.K. Jindal, S. Asija, A. Sharma, Co (II), Ni (II), Cu (II) and Zn (II) complexes of Schiff base ligands: Synthesis, characterization, DFT, in vitro antimicrobial activity and molecular docking studies, *Research on Chemical Intermediates* 49(3) (2023) 939-965.
- [25] E.M. Zayed, M.A. Zayed, H.A. Abd El Salam, G.A. Nawwar, Synthesis, structural characterization, density functional theory (B3LYP) calculations, thermal behaviour, docking and antimicrobial activity of 4-amino-5-(heptadec-8-en-1-yl)-4H-1, 2, 4-triazole-3-thiol and its metal chelates, *Applied Organometallic Chemistry* 32(12) (2018) e4535.
- [26] G. Kanagasabapathy, S. Britto, V. Anbazhagan, Synthesis, characterization and molecular docking studies of highly functionalized and biologically active derivatives of 2-aminothiazole, *Journal of Molecular Structure* 1275 (2023) 134593.
- [27] A.I. Hassaballah, A.K. El-Ziaty, E.F. Ewies, E.M. Zayed, G.G. Mohamed, Synthesis of pyrimidine ligand and its mononuclear metal (II)/(III) complexes: Spectroscopic characterization, thermal, DFT, molecular docking, antimicrobial and anticancer studies, *Inorganic Chemistry Communications* 155 (2023) 110989.
- [28] L.M. Aroua, S.K. Alhag, L.A. Al-Shuraym, S. Messaoudi, J.A. Mahyoub, M.Y. Alfaiji, W.M. Al-Otaibi, Synthesis and characterization of different complexes derived from Schiff base and evaluation as a potential anticancer, antimicrobial, and insecticide agent, *Saudi Journal of Biological Sciences* 30(3) (2023) 103598.
- [29] G. Moustafa, E. Sabry, E.M. Zayed, G.G. Mohamed, Structural characterization, spectroscopic studies, and molecular docking studies on metal complexes of new hexadentate cyclic peptide ligand, *Applied Organometallic Chemistry* 36(2) (2022) e6515.
- [30] S. Daravath, N. Vamsikrishna, N. Ganji, K. Venkateswarlu, Synthesis, characterization, DNA binding ability, nuclease efficacy and biological evaluation studies of Co (II), Ni (II) and Cu (II) complexes with benzothiazole Schiff base, *Chemical Data Collections* 17 (2018) 159-168.
- [31] E.M. Zayed, H.A. Abd ElSallam, M.I. Fathala, F.M. Sroor, Naphthalene-1, 2-dione and indoline-2, 3-dione as Convenient Ligands to Prepare Mixed Ligand Complexes of Mn, Cu And Cd: Synthesis, Spectroscopic Characterization, DFT Study and Antibacterial Activity, *ChemistrySelect* 8(15) (2023) e202300145.
- [32] H.A. Abd El Salam, G.G. Mohamed, E.M. Zayed, Synthesis, spectroscopic characterization, biological application and molecular docking studies of some transition metal complexes of isophthalamide ligand, *Journal of Molecular Structure* 1273 (2023) 134231.
- [33] H.A. Abd El Salam, G. Moustafa, E.M. Zayed, G.G. Mohamed, Isophthaloylbis (azanediy) dipeptide ligand and its complexes: structural study, spectroscopic, molecular orbital, molecular docking, and biological activity properties, *Polycyclic Aromatic Compounds* 43(6) (2023) 4866-4888.
- [34] I. Buta, S. Shova, S. Ilies, F. Manea, M. Andruh, O. Costisor, Mono- and oligonuclear complexes based on a o-vanillin derived Schiff-base ligand: Synthesis, crystal structures, luminescent and electrochemical properties, *Journal of Molecular Structure* 1248 (2022) 131439.
- [35] E.M. Zayed, E.F. Ewies, A.I. Hassaballah, G.G. Mohamed, Synthesis, characterization, DFT, docking, antimicrobial and thermal study of pyrimidine-carbonitrile ligand and its metal complexes, *Journal of Molecular Structure* 1284 (2023) 135396.
- [36] E.M. Zayed, M. Zayed, Synthesis of novel Schiff's bases of highly potential biological activities and their structure investigation, *Spectrochimica Acta Part A: Molecular and Biomolecular Spectroscopy* 143 (2015) 81-90.
- [37] H.A. Abd El Salam, U. Fathy, E.M. Zayed, M.F. El Shehry, a. Ahmed E. Gouda, Design, Synthesis, Cytotoxic Activity and Molecular Docking Studies of Naphthyl Pyrazolyl Thiazole Derivatives as Anticancer Agents, *ChemistrySelect* 8(2) (2023) e202203956.
- [38] E.M. Zayed, M. Zayed, M. El-Desawy, Preparation and structure investigation of

- novel Schiff bases using spectroscopic, thermal analyses and molecular orbital calculations and studying their biological activities, *Spectrochimica Acta Part A: Molecular and Biomolecular Spectroscopy* 134 (2015) 155-164.
- [39] A. Reiss, M.C. Chifiriuc, E. Amzoiu, N. Cioateră, I. Dăbuleanu, P. Rotaru, New metal (II) complexes with ceftazidime Schiff base, *Journal of Thermal Analysis and Calorimetry* 131 (2018) 2073-2085.
- [40] A. Bartyzel, Synthesis, thermal study and some properties of N₂O₄—Donor Schiff base and its Mn (III), Co (II), Ni (II), Cu (II) and Zn (II) complexes, *Journal of Thermal Analysis and Calorimetry* 127 (2017) 2133-2147.
- [41] L. Calu, M. Badea, N. Čelan Korošin, M.C. Chifiriuc, C. Bleotu, N. Stanică, L. Silvestro, M. Maurer, R. Olar, Spectral, thermal and biological characterization of complexes with a Schiff base bearing triazole moiety as potential antimicrobial species, *Journal of Thermal Analysis and Calorimetry* 134 (2018) 1839-1850.